

Complex magnetic phase diagram with a small phase pocket in a three-dimensional frustrated magnet CuInCr₄S₈

M. Gen^{1,2*}, H. Ishikawa¹, A. Ikeda¹, A. Miyake¹, Z. Yang¹, Y. Okamoto³, M. Mori³, K. Takenaka³, T. Kurumaji², Y. Tokunaga², T. Arima², M. Tokunaga¹, K. Kindo¹, Y. H. Matsuda¹, and Y. Kohama¹

¹ *Institute for Solid State Physics, University of Tokyo, Kashiwa 277-8581, Japan*

² *Department of Advanced Materials Science, University of Tokyo, Kashiwa 277-8561, Japan*

³ *Department of Applied Physics, Nagoya University, Nagoya 464-8603, Japan*

*Correspondence is addressed to M.G. (E-mail: gen@edu.k.u-tokyo.ac.jp)

Frustrated magnets with a strong spin-lattice coupling can show rich magnetic phases and the associated fascinating phenomena. A promising platform is the breathing pyrochlore magnet CuInCr₄S₈ with localized $S = 3/2$ Cr³⁺ ions, which is proposed to be effectively viewed as an $S = 6$ Heisenberg antiferromagnet on the face-centered-cubic lattice. Here, we unveil that CuInCr₄S₈ exhibits a complex magnetic phase diagram with a small phase pocket (A-phase) by means of magnetization, magnetostriction, magnetocapacitance, and magnetocaloric-effect measurements in pulsed high magnetic fields of up to 60 T. Remarkably, the appearance of A-phase is accompanied by anomalous magnetostrictive and magnetocapacitive responses, suggesting the emergence of helimagnetism in contrast to the neighboring commensurate magnetic phases. Besides, the high-entropy nature is confirmed in the high-temperature region of A-phase. These features are potentially related to a thermal fluctuation-driven multiple- q state caused by the magnetic frustration, which has been theoretically predicted but yet experimentally undiscovered.

The search for magnetic materials that exhibit a rich magnetic-field-versus-temperature (H - T) phase diagram is a steady but important process in the pursuit of novel magnetic phenomena and emergent functionalities. In external magnetic fields, the competition among several magnetic interactions and/or the interplay between spin and lattice degrees of freedom, i.e., the spin-lattice coupling (SLC), can induce a variety of magnetic states from collinear to noncollinear and noncoplanar magnetic structures. Besides, the thermal fluctuation sometimes has a significant impact on the stability of magnetic orderings. In the triangular or kagomé lattice Heisenberg antiferromagnet, for example, the up-up-down collinear state associated with a 1/3-magnetization plateau is stabilized by the order-by-disorder mechanism [1,2]. Another prominent example is the appearance of topologically nontrivial spin textures with a superposition of multiple spin modulations (multiple- q), as represented by a skyrmion lattice (SkL). The SkL phase has been so far found in a number of materials with a noncentrosymmetric crystal lattice [3-6], where the spin helix is induced by the competition between the ferromagnetic (FM) exchange and Dzyaloshinskii-Moriya (DM) interactions [7,8]. In these cases, the SkL phase exists adjacent to the corresponding single- q phase in the H - T parameter space, and usually appears in a closed H - T regime (often called “A-phase pocket”) [3-6].

Theoretically, thermal fluctuation-driven multiple- q states can appear also in insulating frustrated magnets, such as the SkL (triple- q) in the J_1 - J_3 model on the triangular lattice [9] and the meron/antimeron-like lattice (double- q) in the J_1 - J_2 model on the honeycomb lattice [10,11]. The proposed H - T phase diagrams are rather complicated, similar to those of the DM-induced skyrmion hosts accommodating the A-phase pocket. Although several compounds such as NiGa_2S_4 [12] and $\text{Bi}_3\text{Mn}_4\text{O}_{12}(\text{NO}_3)_2$ [13] are raised as candidates for realizing these theoretical predictions, the verification is a big challenge because experiments in high magnetic fields are often required due to the presence of strong antiferromagnetic (AFM) exchange interactions in real compounds.

Our present target is $\text{CuInCr}_4\text{S}_8$ [14-17], a member of chromium spinels, ACr_2X_4 ($A=\text{Mg}, \text{Zn}, \text{Cd}, \text{Hg}$; $X=\text{O}, \text{S}, \text{Se}$), comprised of a pyrochlore network of $S = 3/2$ Cr^{3+} ions, which are known as the typical three-dimensional insulating frustrated magnets with a strong SLC [18-28]. Here, nonmagnetic Cu^+ and In^{3+} ions are regularly arranged in the A -site of the spinel structure (Fig. 1a). The difference

in their chemical pressure renders the corner-sharing Cr₄ tetrahedra expanding and contracting alternatively, resulting in the so-called breathing pyrochlore lattice with nonequivalent nearest-neighbor (NN) exchange interactions, J and J' , in the small and large tetrahedra, respectively (Fig. 1b) [14,29]. The signs of J and J' depend on the delicate balance between the AFM direct exchange due to the overlapping of t_{2g} orbitals and the FM superexchange via Cr-S-Cr path [21]. Interestingly, the special condition of $J > 0$ (AFM) and $J' < 0$ (FM) is satisfied in CuInCr₄S₈ according to the density-functional-theory calculation, where the exchange parameters are estimated to $J = 14.7$ K, $J' = -26.0$ K, $J_2 = 1.1$ K, $J_{3a} = 6.4$ K, and $J_{3b} = 4.5$ K (Fig. 1b) [17]. Since the FM J' does not compete with any other exchange interactions listed above, magnetic moments on each large Cr₄ tetrahedron behave ferromagnetically at low temperatures, which is observed as the cluster excitation by inelastic neutron scattering [16]. The magnetism of CuInCr₄S₈ can hence be mapped onto $S = 6$ spins on the face-centered-cubic (FCC) lattice with the NN AFM interaction $J_{t1} \equiv J + 4J_2 + 2(J_{3a} + J_{3b}) = 41$ K (Fig. 1c). Since the geometrical frustration remains in this effective FCC lattice, a robust 1/2-magnetization plateau with a 3-up-1-down magnetic structure (C-phase) appears via the exchange-striction mechanism [15], as in Cr spinel oxides [18,20,25,28,31,33,34]. Furthermore, the presence of an intermediate-field phase (Y-phase) in a wide field range between the low-field AFM phase (X-phase) and C-phase is a distinctive feature of this compound, which seems to owe to the peculiar combination of the emergent FCC lattice and the SLC [14,15]. The previous focus on the in-field properties of CuInCr₄S₈ was limited to the ground states [14,15], while the thermal-fluctuation effects on the stability of C- and Y-phases have remained unexplored.

Here, we report on a fascinating H - T phase diagram of CuInCr₄S₈, revealed by means of magnetization, magnetostriction [35], magnetocapacitance [36], and magnetocaloric-effect (MCE) measurements [37] in pulsed high magnetic fields of up to 60 T. The most striking finding is the existence of a small phase pocket (A-phase), which extends from the phase boundary with the paramagnetic phase towards lower temperature and stabilizes instead of Y-phase (Fig. 1d). Remarkably, the transition from X- to A-phase is accompanied by anomalous magnetostrictive and magnetocapacitive responses. These observations suggest the appearance of helimagnetism in A-

phase through a commensurate-to-incommensurate phase transition. Besides, the high-entropy nature is confirmed in the high-temperature region of A-phase. Given the similarity of the obtained H - T phase diagram to that of skyrmion hosts [3-6], the emergence of a multiple- q vortex-like magnetic structure is also possible. The present discovery unveils novel aspects of SLC phenomena as well as paves the way for searching theoretically predicted thermal fluctuation-driven multiple- q states in insulating frustrated magnets.

Results

Magnetic properties of the low-field phase (X-phase)

We first mention notable aspects of the low-field phase (X-phase) of CuInCr₄S₈ reflecting the FCC lattice magnetism. Cr spinels typically undergo a first-order phase transition into an AFM 2-up-2-down collinear structure [20,23,30] or an incommensurate helical structure [22,24] accompanied by the crystal symmetry lowering due to the SLC. For CuInCr₄S₈, the appearance of X-phase is associated with a sudden drop in the magnetic susceptibility M/H at $T_N = 35$ K (Fig. 2a) and a peak in the specific heat C at $T_p = 34$ K (Fig. 2b). However, a recent neutron diffraction study has revealed that the crystal structure remains the cubic $F\bar{4}3m$ symmetry down to 2 K [16]. Our further experiments also support the uniqueness of the low-field magnetic properties of CuInCr₄S₈. The normalized thermal expansion $\Delta L/L_{2K}$ and the dielectric constant ϵ' do not exhibit any sharp anomalies at T_N (Figs. 2c and 2d), unlike other Cr spinels [19,26,28,30,32]. Also, no hysteretic behavior is observed in the M/H - T curve, indicating that the phase transition at T_N is of the second order, and the SLC does not seem to be responsible for the appearance of X-phase.

Let us here discuss the characteristic of X-phase based on the J_{t1} - J_{t2} - J_{t3} model on the effective FCC lattice, where J_{t2} and J_{t3} stand for the 2nd- and 3rd-NN interactions (Fig. 1c). Theoretically, two kinds of commensurate AFM order, Type-I with $\mathbf{q}=(1\ 0\ 0)$ and Type-III with $\mathbf{q}=(1\ \frac{1}{2}\ 0)$, appear at zero field for $J_{t2} < 4J_{t3}$ and $J_{t2} > 4J_{t3}$, respectively, if $|J_{t2}|, |J_{t3}| \ll J_{t1}$ [39]. Note that J_{t2} and J_{t3} arise from the 4th or higher order NN exchange interactions in the original breathing pyrochlore lattice, and should be much weaker than J_{t1} in CuInCr₄S₈. Indeed, Type-I order has been confirmed

for CuInCr₄S₈ by powder neutron diffraction, and the observed magnon dispersion is accountable by incorporating FM J_{t2} (< 0) [16,40]. Although the local spin configuration of X-phase has not been fully identified, an “all-in-all-out”-like one [40] and a coplanar one in which the two AFM spin pairs are canted to each other [16] have been proposed as candidates rather than the 2-up-2-down collinear one. This is curious because the SLC or thermal fluctuation tends to favor a collinear spin configuration out of the continuous degeneracy regarding the directions of four inequivalent spins in Type-I order [41,42]. Moreover, neither of the proposed magnetic structures can be explained just by considering the DM interactions which should exist to a greater or lesser extent in the breathing pyrochlore lattice (Supplementary Note 4) [7,8,43]. We note that a small singularity at T_N and a hump structure around 10 K in the $C/T-T$ curve (Fig. 2b) suggest the existence of a high magnetic entropy even below T_N (Supplementary Note 5). These features are unique to CuInCr₄S₈ among Cr spinels [14,26,27,29] and would stem from the magnetic frustration inherent to the effective FCC lattice Heisenberg antiferromagnet.

Temperature dependence of magnetization, magnetostriction, and magnetocapacitance in pulsed high magnetic fields of up to 60 T

In order to clarify the in-field properties of CuInCr₄S₈ in detail, we measured magnetization, longitudinal magnetostriction, and magnetocapacitance in pulsed high magnetic fields of up to 60 T at various initial temperatures (T_{ini}). All the magnetization and magnetostriction data are summarized in Fig. 3, and some of them are arranged along with the magnetocapacitance data for several selected T_{ini} in Fig. 4. Note that the observed results are irreversible and hysteretic especially for low T_{ini} because of significant sample-temperature changes in the field-descending process, as discussed below. We will hence mainly focus on the data in the field-elevating process, which are useful for constructing the $H-T$ phase diagram (the discussions on the field-descending process are given in Supplementary Note 6).

For the lowest T_{ini} of 1.4 K, two-step metamagnetic transitions take place at $\mu_0 H_{c1} = 32$ T and $\mu_0 H_{c2} = 56$ T (Fig. 3a), followed by a 1/2-magnetization plateau which continues up to $\mu_0 H_{c3} \approx 110$ T [15].

Correspondingly, a substantial lattice expansion is observed at H_{c1} and H_{c2} (Fig. 3c), suggesting the importance of the SLC on these phase transitions. As discussed in Ref. [15], the overall magnetization curve can be roughly reproduced by the minimal Hamiltonian incorporating the SLC, which effectively produces the biquadratic exchange term $-(\mathbf{S}_i \cdot \mathbf{S}_j)^2$ between NN spins [33,34]. According to this, the spin configurations within each small tetrahedron in the low-field X-phase, the intermediate-field Y-phase between H_{c1} and H_{c2} , and C-phase with the 1/2-plateau can be assigned to the canted 2:2, canted 2:1:1, and collinear 3-up-1-down state, respectively (Fig. 1e). As T_{ini} increases, each critical field is gradually decreased. The hump structures at H_{c2} in dM/dH and dL/dH become blunt for $T_{\text{ini}} \geq 20$ K, making the phase boundary indiscernible (Figs. 3b and 3d). For $T_{\text{ini}} \geq 35$ K ($=T_N$), the transition from the paramagnetic to the field-induced ordered phase is observed. The critical field H_P becomes higher on increasing T_{ini} up to 50 K, suggesting that C-phase is stabilized by the thermal fluctuation and may extend to a higher temperature region. A moderate magnetocapacitance change is also seen at the transition into C-phase for $T_{\text{ini}} \geq 10$ K (Figs. 4f, 4i, 4l, and 4o), which may be attributed to the local lattice distortion to stabilize the 3-up-1-down magnetic structure via the exchange-striction mechanism.

Magnetostrictive and magnetocapacitive effects in the A-phase pocket

In addition to the previously reported X-, Y-, and C-phases, a novel field-induced phase (A-phase) is found in the series of high-field experiments. Let us here focus on the magnetization and magnetostriction curves for an intermediate T_{ini} range between 10 and 35 K. Taking a closer look at Fig. 3a, one can notice that the lowest-field metamagnetic transition becomes exceptionally steep for $T_{\text{ini}} = 10$ K, which is clearly shown as the peak sharpness in the dM/dH curve (Fig. 3b). This is reflected in the plot of magnetization-versus-temperature at 35 T showing a maximum at 10 K (inset in Fig. 3b). Besides, a dip structure of $\Delta L/L_{0T}$ appears in a narrow field region for $10 \text{ K} \leq T_{\text{ini}} \leq 30$ K (inset in Fig. 3c). These features suggest that the nature of the lowest-field metamagnetic transition changes across $T_{\text{ini}} = 10$ K. Accordingly, the critical field above 10 K should be distinguished from H_{c1} and instead termed H_{A1} . Importantly, another tiny dM/dH peak appears at around the midpoint between

H_{A1} and H_{c2} (termed H_{A2}) for $T_{\text{ini}} = 10$ K, developing toward higher T_{ini} up to 32.5 K (Fig. 3a). An anomaly is also visible at H_{A2} in the $\Delta L/L_{0T}$ data for $20 \text{ K} \leq T_{\text{ini}} \leq 30$ K (Fig. 3c). These observations indicate the existence of another phase intervened between X- and Y-phases.

According to the microscopic magnetoelastic theory [28], the classical Heisenberg antiferromagnet on the regular pyrochlore lattice exhibits a volume expansion, equivalently a positive magnetostriction, proportional to M^2 during the successive field-induced phase transitions until saturation, when assuming a constant 16-sublattice magnetic unit cell. This tendency is roughly seen in the $\Delta L/L_{0T}$ data of CuInCr₄S₈ below 10 K (Figs. 3a and 3c), where $\Delta L/L_{0T}$ follows a parabolic field-dependence within X-phase and smoothly increases even across the phase transitions at H_{c1} and H_{c2} . This suggests that the magnetic unit cells in Y- and C-phases remain unchanged as in X-phase. From this viewpoint, the observed dip structure of $\Delta L/L_{0T}$ for $12 \text{ K} \leq T_{\text{ini}} \leq 30$ K is unusual. The negative magnetostriction is not seen within A-phase, but occurs as a precursor to the metamagnetic transition from X- to A-phase at H_{A1} (Figs. 4g, 4h, 4j, and 4k). We infer that such a nonmonotonic $\Delta L/L_{0T}$ behavior would arise from the modification of the magnetic unit cell, i.e., the reconstruction of q -vector.

Interestingly, it is uncovered that A-phase is associated with a substantial magnetodielectric coupling in addition to the anomalous magnetostrictive behavior. No signature of a magnetocapacitance change is observed at H_{c1} within our experimental resolution for $T_{\text{ini}} = 4.2$ K (Fig. 4c), while the magnetocapacitance is suddenly enhanced by ~0.3 % at H_{A1} for $T_{\text{ini}} = 10$ K (Fig. 4f), which is exactly the characteristic temperature of the appearance of A-phase. Such a magnetocapacitive response is visible also for $T_{\text{ini}} = 15$ and 25 K (Figs. 4i and 4l), signaling the emergence of multiferroicity in A-phase originating from the helical spin modulation [44,45].

Sample temperature change in our experimental condition with millisecond pulsed-field duration

All the aforementioned measurements were performed under the nonadiabatic condition by immersing the sample in ⁴He liquid or gas. However, the heating or cooling effects of the sample are usually non-negligible in millisecond pulsed-field experiments. Accordingly, we measured the sample

temperature $T(H)$ in pulsed magnetic fields of up to 60 T under the nonadiabatic condition at $T_{\text{ini}} = 4.2$ K. Surprisingly, $T(H)$ was found to drastically increase by more than 10 K at H_{C2} in the field-elevating process, possibly due to the hysteresis loss accompanied by the first-order phase transition into C-phase (Fig. 5a). Since the thermal equilibrium was not sufficiently achieved around the maximum field, the sample was not cooled down below 10 K in the field-descending process. Here, successive phase transitions more complicated than those from C-, Y-, A-, to X-phase would take place, judging from at least three anomalies in the $T(H)$ curve in the field-descending process (see also Supplementary Note 6). Note that such a strong heating effect does not seem to occur in the magnetization measurements at $T_{\text{ini}} = 1.4$ and 4.2 K because the magnetization curves in the field-descending process are less hysteretic and no double-hump structure is seen in the dM/dH curves around 25 T unlike for $T_{\text{ini}} \geq 7.5$ K (Figs. 3a, b, and 4a). The difference in the degree of the heating effect might be due to the sample form as well as the thermal bath environment; powder samples were used for the magnetization measurements, whereas sintered samples for other measurements. We stress that a nearly isothermal condition is confirmed below H_{C2} for all the measurements at $T_{\text{ini}} = 4.2$ K. This would be applicable also for $T_{\text{ini}} > 4.2$ K because the heating effect becomes less pronounced for higher T_{ini} as shown next. Thus, it would be reasonable to use all the data in the field-elevating process for mapping out the H - T phase diagram (Fig. 1d).

Magnetic entropy changes through successive phase transitions

In order to extract information about the magnetic entropy (S_M) in each phase, we further investigated the magnetocaloric effect (MCE) under the adiabatic condition. The MCE is the sample-temperature change induced by the evolution of S_M upon the application or removal of an external magnetic field. When there is no irreversible first-order transition, the obtained $T(H)$ curve can be regarded as the isentropic curve. As a consequence, the S_M increase (decrease) is detected as the $T(H)$ decrease (increase) [37].

For $T_{\text{ini}} \leq T_N$, no apparent $T(H)$ change is observed below $H_{\text{c}1}$ or $H_{\text{A}1}$ (Figs. 5b and 5c), indicating that there is almost no S_M change in X-phase upon the application of a magnetic field. Considering the magnetocaloric relation fulfilled under the isentropic condition

$$\left(\frac{\partial T}{\partial H}\right)_S = -\frac{T}{C_H} \left(\frac{\partial M}{\partial T}\right)_H, \quad (1)$$

where C_H is the specific heat at the constant magnetic field, this observation is compatible with the M/H - T data at 7 T showing a slight temperature dependence below T_N (Fig. 2a). For $T_{\text{ini}} = 5$ and 8 K, however, the $T(H)$ curves show a dramatic increase above $H_{\text{c}1}$ and eventually overlap with each other around the maximum field (Fig. 5b). Those in field-descending processes are completely irreversible, indicating that the contribution of the hysteresis loss is larger than that of an intrinsic MCE in this temperature range. Importantly, an additional $T(H)$ kink is observed at $H_{\text{A}0}$ just above $H_{\text{c}1}$, possibly indicating the phase transition from Y- to A-phase (see dashed gray lines in Fig. 5b). By drawing the $T(H)$ curves in field-elevating processes on the H - T phase diagram, it can be seen that $T(H)$ significantly increases within A-phase (Fig. 5d). Bearing $(\partial M / \partial T)_H < 0$ just above 10 K at around 35 T (inset in Fig. 3b) and Eq. (1) in mind, this would reflect the intrinsic entropy reduction in the low-temperature region of A-phase.

As T_{ini} increases, the $T(H)$ change at $H_{\text{A}1}$ and the accompanying hysteresis become smaller, assuring the achievement of the quasi-isentropic condition (Fig. 5c). Notably, the $T(H)$ behaviors for $20 \text{ K} \leq T_{\text{ini}} \leq 32 \text{ K}$ are qualitatively different from those for $T_{\text{ini}} = 12$ and 16 K; the inflection point at $H_{\text{A}1}$ disappears for the former, indicating that S_M in A-phase is as high as that in X-phase above 20 K (we note again that a high S_M remains in X-phase as discussed in Supplementary Note 5). This implies that A-phase is further subdivided into two phases: e.g., the low- S_M single- q and high- S_M multiple- q phases on the low- and high-temperature regions, respectively. A similar high- S_M nature of the SkL phase (multiple- q) has been experimentally demonstrated by analyzing the magnetization data based on the magnetocaloric relation Eq. (1) [5].

At the transitions from Y- and the paramagnetic phases to C-phase, $T(H)$ commonly starts rising for all the T_{ini} because of the low- S_M nature in the 3-up-1-down collinear magnetic structure (Figs. 5b and

5c). These observations are helpful for determining the phase boundary, especially between Y- and C-phases (denoted by rightward open triangles in Fig. 5d).

Discussion

We have unveiled an exotic H - T phase diagram of the new-type Cr spinel $\text{CuInCr}_4\text{S}_8$ characterized by A-phase appearing in the closed H - T regime around 25-40 T and 10-35 K. Remarkably, the appearance of A-phase is associated with anomalous magnetostrictive and magnetocapacitive responses, suggesting the manifestation of helimagnetism in contrast to the neighboring commensurate magnetic phases. Although the perfect theoretical description which can reproduce the H - T phase diagram of $\text{CuInCr}_4\text{S}_8$ is elusive at this stage, we propose one possible route to the appearance of the A-phase. In all the observed field-induced phase transitions, local lattice distortions as well as the lattice constant change should take place. This induces the modulation of the strengths of J and J' from bond to bond: e.g., the trigonal distortion produces three $J(1 + \delta_1)$ and three $J(1 - \delta_2)$ per one small tetrahedron in the 3-up-1-down collinear state. It has been theoretically suggested that the introduction of tetragonal or trigonal distortions into the FCC lattice with the J_{t1} - J_{t2} model can induce incommensurate helical orders at zero field (Fig. 1c) [46]. This may be related to the observed in-field properties of CuInC_4S_8 ; the lattice distortion would lead to the competition between commensurate Y- and incommensurate A-phases, and the latter is stabilized on the higher temperature side by the entropy effect.

The obtained H - T phase diagram is reminiscent of that of skyrmion host materials with a noncentrosymmetric crystal lattice, characterized by the A-phase pocket [3-6]. In most of the insulating skyrmion hosts discovered so far, the SkL phase originates from the competition between FM and DM interactions, as represented by Cu_2OSeO_3 [4,6]. To the best of our knowledge, there have been no reports on the H - T phase diagram dressed with a distinctive A-phase pocket in insulating frustrated magnets, even though there exist several theoretical predictions on the realization of thermal fluctuation-driven multiple- q states caused by the magnetic frustration [9-11]. Only recently, MnSc_2S_4 , characterized by the J_1 - J_2 - J_3 model on the centrosymmetric diamond lattice, has been found to

exhibit a fractional antiferromagnetic SkL, which seems to be attributed to the anisotropic exchange couplings and is stabilized even at zero temperature [47]. It would be of particular interest whether or not the multiple- q state is realized within A-phase of CuInCr₄S₈. We note that the assignment of A-phase in the present work is tentative, and it may be further subdivided into low- and high-temperature phases, as implied from the magnetoentropic signatures. It is necessary to perform NMR or neutron scattering experiments on single crystals, which are left for future work. Further theoretical investigations are also desired to verify our proposed scenario.

Methods

Sample preparation.

The magnetic long-range ordering temperatures of CuInCr₄S₈ reported so far are ranging from 26 K to 35 K [16,48-50]. Our previous polycrystalline samples (Sample #2) exhibit a magnetic phase transition at $T_N \approx 32$ K [14], which is slightly different from any values reported by other groups. Accordingly, we prepared new polycrystalline batches (Sample #1) by the solid state reaction as in Ref. [14], and found the higher transition temperature as $T_N \approx 35$ K, in accordance with that reported in Refs. [16,49].

Sample characterization.

To compare the sample quality between Samples #1 and #2, powder X-ray diffraction (XRD) patterns were obtained using a commercial X-ray diffractometer (SmartLab, Rigaku), confirming the cubic $F\bar{4}3m$ structure with no detectable impurity for both the samples (Supplementary Note 1). Since no obvious difference was observed in their XRD patterns, it was impossible to evaluate which sample contains less crystallographic disorder and/or defects in the nonmagnetic Cu⁺ and In³⁺ sites and the ligand S²⁻ sites. A series of high-field experiments revealed that field-induced phase transitions are much sharper in Sample #1 than in Sample #2, suggesting that Sample #1 is of higher quality, i.e., the Cr-based pyrochlore network may be better *breathing*. The results for Sample #1 are shown in the main text, while those for Sample #2 are displayed in Supplementary Notes 2 and 3.

Magnetization measurements.

Magnetization up to 7 T was measured using a commercial magnetometer (MPMS, Quantum Design). Magnetization up to ~60 T was measured by the conventional induction method using a coaxial pickup coil in a non-destructive (ND) pulsed magnet (~4 ms duration) at the Institute for Solid State Physics (ISSP), University of Tokyo, Japan.

Thermal expansion and magnetostriction measurements.

Longitudinal magnetostriction up to ~60 T was measured by the optical fiber-Bragg-grating (FBG) technique in a ND pulsed magnet (~36 ms duration) at ISSP [35]. The fiber was adhered to a rod-shaped sintered sample by epoxy Styccast1266. The distortion $\Delta L/L$ was detected by the optical filter method with a resolution of $\sim 10^{-6}$. The thermal expansion at zero field was measured using the same setup during a natural temperature rise from 2 to 60 K.

Dielectric constant and magnetocapacitance measurements.

Dielectric constant at zero field was measured at a frequency of 10 kHz by using an LCR meter (E4980A, Agilent) in a commercial cryostat equipped with a superconducting magnet (PPMS, Quantum Design). Magnetocapacitance up to ~60 T was measured along the field direction at a frequency of 50 kHz by using a capacitance bridge (1615-A, General Radio) in a ND pulsed magnet (~36 ms duration) at ISSP [36]. Silver paste was painted on the top and bottom surfaces to form electrodes for a disk-shaped sintered sample.

Heat capacity and magnetocaloric effect measurements.

Heat capacity at zero field was measured by the thermal relaxation method using a PPMS. The magnetocaloric effect up to ~60 T was measured under both the nonadiabatic and adiabatic conditions in a ND pulsed magnet (~36 ms duration) at ISSP. A sensitive Au₁₆Ge₈₄ film thermometer was sputtered on the surface of a disk-shaped sintered sample, which was calibrated by a commercial Cernox 1030 thermometer [37].

Data availability.

The data sets generated during and/or analyzed during the current study are available from the corresponding author on reasonable request.

Acknowledgements

The authors are grateful for helpful discussions with S. Gao. The authors thank S. Kitani for providing the raw data of the specific heat of CdCr₂O₄ in Ref. [26], which is useful for discussions in the present work (Supplementary Note 5). This work was financially supported by the JSPS KAKENHI Grants-In-Aid for Scientific Research (No. 19H05823, No. 20J10988, and No. 20K20892) and Basic Science Program No. 18-001 of Tokyo Electric Power Company (TEPCO) memorial foundation. M.G. was supported by the JSPS through a Grant-in-Aid for JSPS Fellows.

Author Contributions

M.G. and Y.K. conceived the project. Polycrystalline samples were synthesized by M.G. and M.M. under the supervision of T.K., Y.T., T.A., Y.O. and K.T. The experiments using MPMS/PPMS were performed by M.G. High-field magnetization measurements were performed by H.I. and M.G under the supervision of K.K. High-field magnetostriction measurements were performed by M.G. and A.I. under the supervision of Y.H.M. High-field magnetocapacitance measurements were performed by A.M. and M.G under the supervision of M.T. High-field magnetocaloric effect measurements were performed by M.G. and Z.Y. under the supervision of Y.K. M.G. wrote the manuscript with input comments from all co-authors.

Additional Information

Supplementary Information accompanies this article.

Competing interests: The authors declare no competing financial interests.

References

- [1] Kawamura, H. & Miyashita, S. Phase Transition of the Heisenberg Antiferromagnet on the Triangular Lattice in a Magnetic Field. *J. Phys. Soc. Jpn.* **54**, 4530-4538 (1985).
- [2] Zhitomirsky, M. E. Field-Induced Transitions in a Kagomé Antiferromagnet. *Phys. Rev. Lett.* **88**, 057204 (2002).
- [3] Mühlbauer, S., Binz, B., Jonietz, F., Pfleiderer, C., Rosch, A., Neubauer, A., Georgii, R. & Böni, P. Skyrmiion Lattice in a Chiral Magnet. *Science* **323**, 915-919 (2009).
- [4] Seki, S., Yu, X. Z., Ishiwata, S. & Tokura, Y. Observation of Skyrmions in a Multiferroic Material. *Science* **336**, 198-201 (2012).
- [5] Bocarsly, J. D., Need, R. F., Seshadri, R. & Wilson, S. D. Magnetoentropic signatures of skyrmionic phase behavior in FeGe. *Phys. Rev. B* **97**, 100404(R) (2018).
- [6] Tokura, Y. & Kanazawa, N. Magnetic Skyrmion Materials. *Chem. Rev.* **121**, 2857-2897 (2021).
- [7] Dzyaloshinskii, I. A thermodynamic theory of “weak” ferromagnetism of antiferromagnetics. *J. Phys. Chem. Solids* **4**, 241-255 (1958).
- [8] Moriya, T., New Mechanism of Anisotropic Superexchange Interaction. *Phys. Rev. Lett.* **4**, 228 (1960).
- [9] Okubo, T., Chung, S. & Kawamura, H. Multiple- q States and the Skyrmiion Lattice of the Triangular-Lattice Heisenberg Antiferromagnet under Magnetic Fields. *Phys. Rev. Lett.* **108**, 017206 (2012).
- [10] Shimokawa, T. & Kawamura, H. Ripple State in the Frustrated Honeycomb-Lattice Antiferromagnet. *Phys. Rev. Lett.* **123**, 057202 (2019).
- [11] Shimokawa, T., Okubo, T. & Kawamura, H. Multiple- q states of the J_1 - J_2 classical honeycomb-lattice Heisenberg antiferromagnet under a magnetic field. *Phys. Rev. B* **100**, 224404 (2019).
- [12] Nakatsuji, S., Nambu, Y., Tonomura, H., Sakai, O., Jonas, S., Broholm, C., Tsunetsugu, H., Qiu, Y. & Maeno, Y. Spin Disorder on a Triangular Lattice. *Science* **309**, 1697-1700 (2005).
- [13] Smirnova, O., Azuma, M., Kumada, N., Kusano, Y., Matsuda, M., Shimakawa, Y., Takei, T., Yonesaki, Y. & Kinomura, N. Synthesis, Crystal Structure, and Magnetic Properties of $\text{Bi}_3\text{Mn}_4\text{O}_{12}(\text{NO}_3)_2$ Oxynitrate Comprising $S = 3/2$ Honeycomb Lattice. *J. Am. Chem. Soc.* **131**, 8313-8317 (2009).
- [14] Okamoto, Y., Mori, M., Katayama, N., Miyake, A., Tokunaga, M., Matsuo, A., Kindo, K. & Takenaka, K. Magnetic and Structural Properties of A-Site Ordered Chromium Spinel Sulfides: Alternating Antiferromagnetic and Ferromagnetic Interactions in the Breathing Pyrochlore Lattice. *J. Phys. Soc. Jpn.* **87**, 034709 (2018).
- [15] Gen, M., Okamoto, Y., Mori, M., Takenaka, K. & Kohama, Y. Magnetization process of the breathing pyrochlore magnet $\text{CuInCr}_4\text{S}_8$ in ultrahigh magnetic fields up to 150 T. *Phys. Rev. B* **101**, 054434 (2020).
- [16] Gao, S., May, A. F., Du, M.-H., Paddison, J. A. M., Arachchige, H. S., Pokharel, G., Cruz, C. dela, Zhang, Q., Ehlers, G., Parker, D. S., Mandrus, D. G., Stone, M. B. & Christianson, A. D. Hierarchical excitations from correlated spin tetrahedra on the breathing pyrochlore lattice. *Phys. Rev. B* **103**, 214418 (2021).
- [17] Ghosh, P., Iqbal, Y., Müller, T., Thomale, R., Reuther, J., Gingras, M. J. P. & Jeschke, H. O. Breathing chromium spinels: a showcase for a variety of pyrochlore Heisenberg Hamiltonians. *npj Quantum Mater.* **4**, 63 (2019).

- [18] Ueda, H., Mitamura, H., Goto, T. & Ueda, Y., Successive field-induced transitions in a frustrated antiferromagnet HgCr_2O_4 . *Phys. Rev. B* **73**, 094415 (2006).
- [19] Hemberger, J., Krug von Nidda, H.-A., Tsurkan, V. & Loidl, A., Large Magnetostriiction and Negative Thermal Expansion in the Frustrated Antiferromagnet ZnCr_2Se_4 . *Phys. Rev. Lett.* **98**, 147203 (2007).
- [20] Matsuda, M., Ueda, H., Kikkawa, A., Tanaka, Y., Katsumata, K., Narumi, Y., Inami, T., Ueda, Y. & Lee, S.-H. Spin-lattice instability to a fractional magnetization state in the spinel HgCr_2O_4 . *Nat. Phys.* **3**, 397-400 (2007).
- [21] Yaresko, A. N. Electronic band structure and exchange coupling constants in $A\text{Cr}_2X_4$ spinels ($A=\text{Zn}, \text{Cd}, \text{Hg}; X=\text{O}, \text{S}, \text{Se}$). *Phys. Rev. B* **77**, 115106 (2008).
- [22] Murakawa, H., Onose, Y., Ohgushi, K., Ishiwata, S. & Tokura, Y. Generation of Electric Polarization with Rotating Magnetic Field in Helimagnet ZnCr_2Se_4 . *J. Phys. Soc. Jpn.* **77**, 043709 (2008).
- [23] Ji, S., Lee, S.-H., Broholm, C., Koo, T. Y., Ratcliff, W., Cheong, S.-W. & Zschack, P. Spin-Lattice Order in Frustrated ZnCr_2O_4 . *Phys. Rev. Lett.* **103**, 037201 (2009).
- [24] Tsurkan, V., Zherlitsyn, S., Felea, V., Yasin, S., Skourski, Yu., Deisenhofer, J., Krug von Nidda, H.-A., Lemmens, P., Wosnitza, J. & Loidl, A. Magnetostructural Transitions in a Frustrated Magnet at High Fields. *Phys. Rev. Lett.* **106**, 247202 (2011).
- [25] Miyata, A., Ueda, H., Ueda, Y., Sawabe, H. & Takeyama, S. Magnetic Phases of a Highly Frustrated Magnet, ZnCr_2O_4 , up to an Ultrahigh Magnetic Field of 600 T. *Phys. Rev. Lett.* **107**, 207203 (2011).
- [26] Kitani, S., Tachibana, M., Taira, N. & Kawaji, H. Thermal study of the interplay between spin and lattice in CoCr_2O_4 and CdCr_2O_4 . *Phys. Rev. B* **87**, 064402 (2013).
- [27] Kemei, M. C., Barton, P. T., Moffitt, S. L., Gaulois, M. W., Kurzman, J. A., Seshadri, R., Suchomel, M. R. & Kim, Y. Crystal structures of spin Jahn-Teller-ordered MgCr_2O_4 and ZnCr_2O_4 . *J. Phys.: Condens. Matter* **25**, 326001 (2013).
- [28] Rossi, L., Bobel, A., Wiedmann, S., Küchler, R., Motome, Y., Penc, K., Shannon, N., Ueda, H. & Bryant, B. Negative Thermal Expansion in the Plateau State of a Magnetically Frustrated Spinel. *Phys. Rev. Lett.* **123**, 027205 (2019).
- [29] Okamoto, Y., Nilsen, G. J., Attfield, J. P. & Hiroi, Z., Breathing Pyrochlore Lattice Realized in A -Site Ordered Spinel Oxides $\text{LiGaCr}_4\text{O}_8$ and $\text{LiInCr}_4\text{O}_8$. *Phys. Rev. Lett.* **110**, 097203 (2013).
- [30] Saha, R., Fauth, F., Avdeev, M., Kayser, P., Kennedy, B. J. & Sundaresan A. Magnetodielectric effects in A -site cation-ordered chromate spinels $\text{Li}M\text{Cr}_4\text{O}_8$ ($M=\text{Ga}$ and In). *Phys. Rev. B* **94**, 064420 (2016).
- [31] Gen, M., Nakamura, D., Okamoto, Y. & Takeyama, S. Ultra-high magnetic field magnetic phases up to 130 T in a breathing pyrochlore antiferromagnet $\text{LiInCr}_4\text{O}_8$. *J. Magn. Magn. Mater.* **473**, 387-393 (2019).
- [32] Kanematsu, T., Mori, M., Okamoto, Y., Yajima, T. & Takenaka, K. Thermal Expansion and Volume Magnetostriiction in Breathing Pyrochlore Magnets $\text{Li}A\text{Cr}_4X_8$ ($A=\text{Ga}, \text{In}, X=\text{O}, \text{S}$). *J. Phys. Soc. Jpn.* **89**, 073708 (2020).
- [33] Penc, K., Shannon, N. & Shiba, H. Half-Magnetization Plateau Stabilized by Structural Distortion in the Antiferromagnetic Heisenberg Model on a Pyrochlore Lattice. *Phys. Rev. Lett.* **93**, 197203 (2004).
- [34] Aoyama, K., Gen, M. & Kawamura, H. Effects of spin-lattice coupling and a magnetic field in classical Heisenberg antiferromagnets on the breathing pyrochlore lattice. *Phys. Rev. B* **104**, 184411 (2021).

- [35] Ikeda, A., Matsuda, Y. H. & Tsuda, H. Note: Optical filter method for high-resolution magnetostriction measurement using fiber Bragg grating under millisecond-pulsed high magnetic fields at cryogenic temperatures. *Rev. Sci. Instrum.* **89**, 096103 (2018).
- [36] Miyake, A., Mitamura, H., Kawachi, S., Kimura, K., Kimura, T., Kihara, T., Tachibana, M. & Tokunaga, M. Capacitive detection of magnetostriction, dielectric constant, and magneto-caloric effects in pulsed magnetic fields. *Rev. Sci. Instrum.* **91**, 105103 (2020).
- [37] Kihara, T., Kohama, Y., Hashimoto, Y., Katsumoto, S. & Tokunaga, M. Adiabatic measurements of magneto-caloric effects in pulsed magnetic fields up to 55 T. *Rev. Sci. Instrum.* **84**, 074901 (2013).
- [38] Momma, K. & Izumi, F. VESTA 3 for three-dimensional visualization of crystal, volumetric and morphology data. *J. Appl. Cryst.* **44**, 1272-1276 (2011).
- [39] Balla, P., Iqbal, Y. & Penc, K. Degenerate manifolds, helimagnets, and multi-Q chiral phases in the classical Heisenberg antiferromagnet on the face-centered-cubic lattice. *Phys. Rev. Res.* **2**, 043278 (2020).
- [40] Plumier, R., Lotgering, F. K. & Stapele, R. P. Magnetic properties of $\text{Cu}_{1/2}\text{In}_{1/2}\text{Cr}_2\text{S}_4$ and some related compounds. *J. Phys. C* **1**, 324-325 (1971).
- [41] Henley, C. L. Ordering by disorder: Ground-state selection in fcc vector antiferromagnets. *J. Appl. Phys.* **61**, 3962-3964 (1987).
- [42] Benton, O. & Shannon, N. Ground State Selection and Spin-Liquid Behavior in the Classical Heisenberg Model on the Breathing Pyrochlore Lattice. *J. Phys. Soc. Jpn.* **84**, 104710 (2015).
- [43] Elhajal, M., Canals, B., Sunyer, R. & Lacroix, C. Ordering in the pyrochlore antiferromagnet due to Dzyaloshinsky-Moriya interactions. *Phys. Rev. B* **71**, 094420 (2005).
- [44] Katsura, H., Nagaosa, N. & Balatsky, A. V. Spin Current and Magnetoelectric Effect in Noncollinear Magnets. *Phys. Rev. Lett.* **95**, 057205 (2005).
- [45] Arima, T. Ferroelectricity Induced by Proper-Screw Type Magnetic Order, *J. Phys. Soc. Jpn.* **76**, 073702 (2007).
- [46] Yamamoto, Y. & Nagamiya, T. Spin Arrangements in Magnetic Compounds of the Rocksalt Crystal Structure. *J. Phys. Soc. Jpn.* **32**, 1248-1261 (1972).
- [47] Gao, S., Rosales, H. D., Albarracín, F. A. G., Tsurkan, V., Kaur, G., Fennell, T., Steffens, P., Boehm, M., Čermák, P., Schneidewind, A., Ressouche, E., Cabra, D. C., Rüegg, C. & Zaharko, O. Fractional antiferromagnetic skyrmion lattice induced by anisotropic couplings. *Nature* **586**, 37-41 (2020).
- [48] Pinch, H. L., Woods, M. J. & Lopatin, E. Some new mixed A-site chromium chalcogenide spinels. *Mat. Res. Bull.* **5**, 425-430 (1970).
- [49] Plumier, R., Sougi, M., Lecomte, M. & Miedan-Gros, A. High Magnetic Field Study of Sulphur Spinel $\text{Cu}_{1/2}\text{In}_{1/2}\text{Cr}_2\text{S}_4$. *Z. Phys. B* **40**, 227-231 (1980).
- [50] Aminov, T. G., Shabunina, G. G., Busheva, E. V. & Novotortsev, V. M. Magnetic Properties of $\text{Co}_x(\text{Cu}_{0.5}\text{In}_{0.5})_{1-x}\text{Cr}_2\text{S}_4$ Solid Solutions. *Russ. J. Inorg. Chem.* **61**, 461-469 (2016).

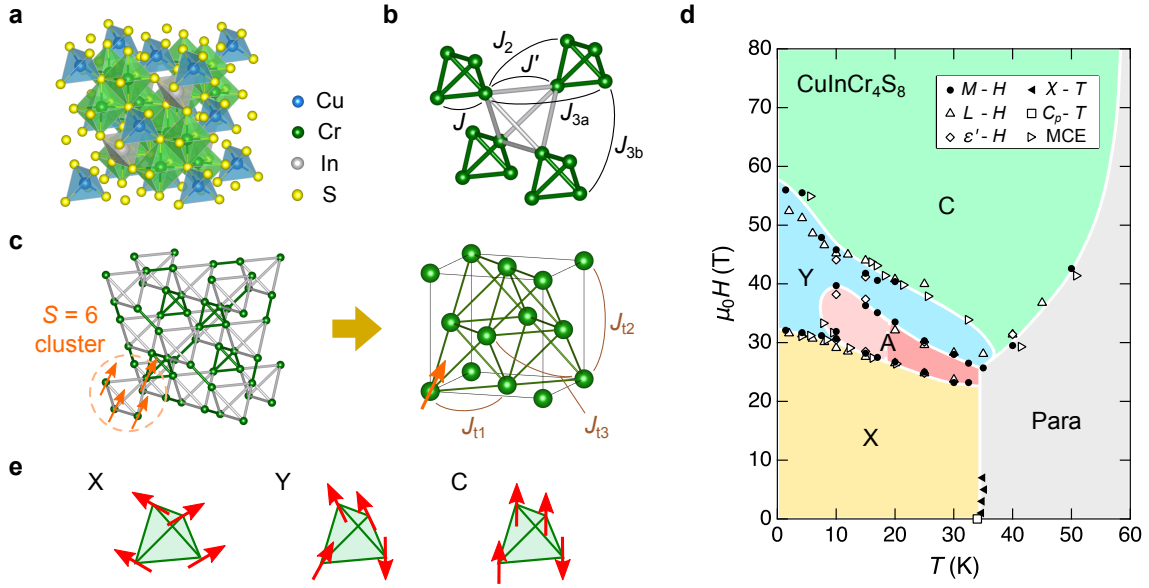


Fig. 1: Magnetic model and phase diagram of CuInCr₄S₈. (a) Crystal structure of CuInCr₄S₈ [14]. (b) Breathing pyrochlore lattice comprised of magnetic Cr³⁺ ions with two kinds of the NN exchange interactions, J and J' , in the small and large tetrahedra, respectively, and further-neighbor exchange interactions up to the 3rd-NN. (c) Effective magnetic model of CuInCr₄S₈ mapped on the face-centered-cubic lattice with the NN AFM exchange interaction $J_{t1} \equiv J + 4J_2 + 2(J_{3a} + J_{3b})$. (d) Magnetic-field-versus-temperature phase diagram of CuInCr₄S₈ derived from a series of experiments in the present work. Judging from the magnetoentropic signatures, A-phase is possibly further subdivided into two distinct phases in the low- (pink) and high-temperature regions (red). (e) Schematic of the magnetic structures of X-, Y-, and C-phases predicted by the previous magnetoelastic theory [15]. The illustrations in (a-c) are drawn by VESTA software [38].

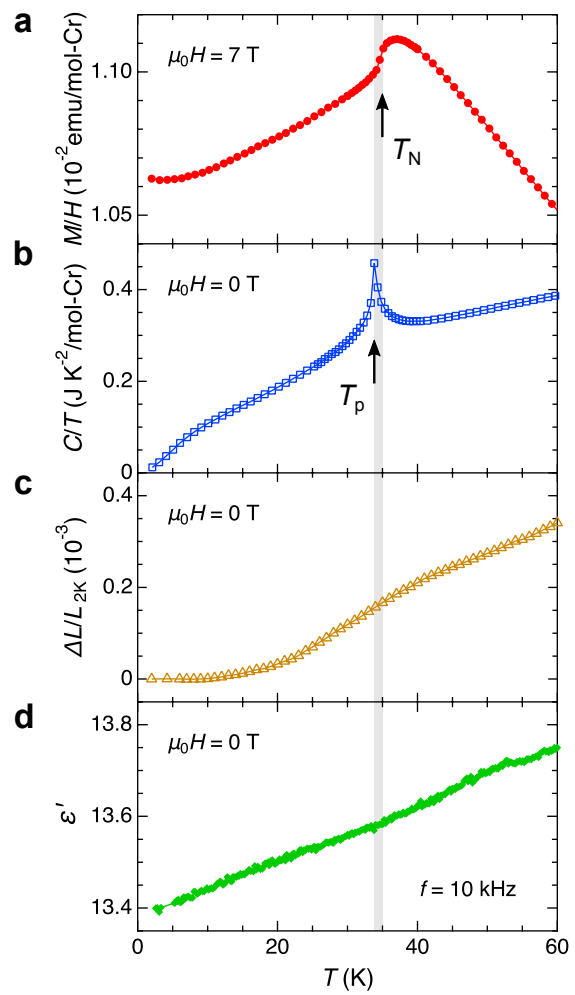


Fig. 2: Temperature dependence of physical properties of CuInCr₄S₈. (a) Magnetization measured at 7 T after zero-field cooling. (b) Specific heat divided by temperature at 0 T. (c) Thermal expansion compared to the 2-K data at 0 T. (d) Dielectric constant at a frequency of 10 kHz at 0 T. All the measurements were performed in a warming process.

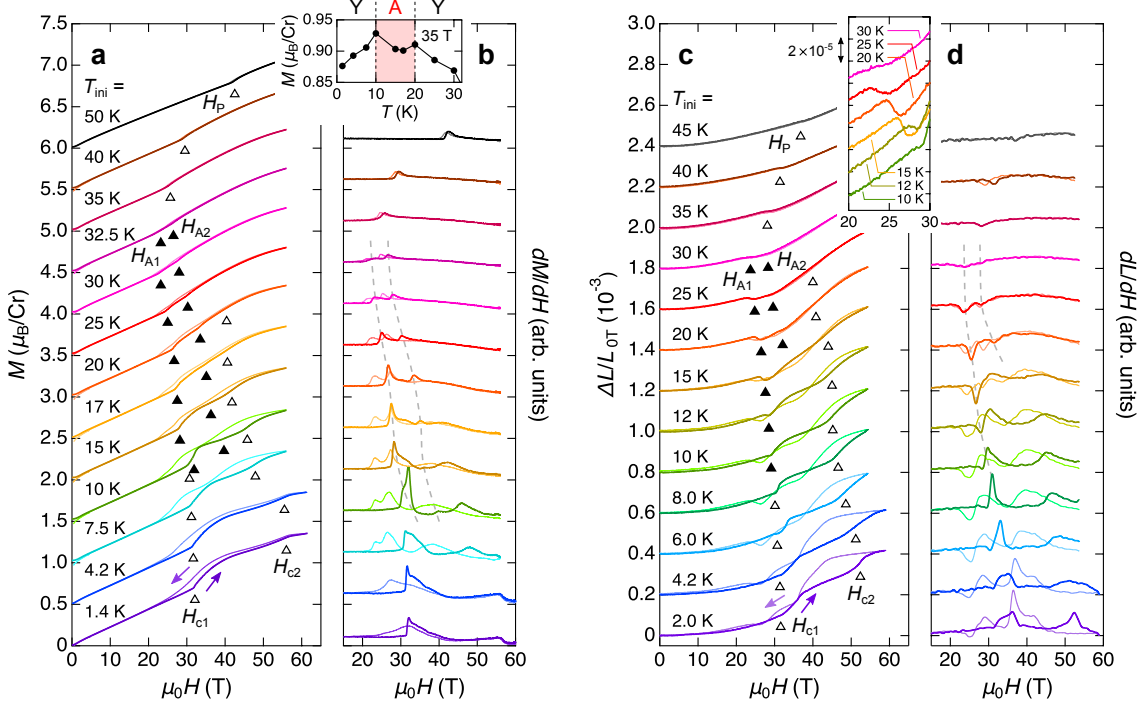


Fig. 3: Magnetic-field induced successive phase transitions in CuInCr₄S₈. (a) Magnetization, (b) its field-derivative, (c) longitudinal magnetostriction, and (d) its field-derivative as a function of magnetic field measured at various initial temperatures T_{ini} . The thick (thin) lines correspond to the data in field-elevating (descending) processes. All the data except for the lowest-temperature one are shifted upward for clarity. The inset in (b) is a magnetization-versus-temperature plot at 35 T. The inset in (c) shows the enlarged view of the magnetostriction curves in field-elevating processes for $10 \leq T_{\text{ini}} \leq 30 K, where lattice shrinkage occurs as the precursor of the phase transition from X- to A-phase at $H_{\text{A}1}$. The filled (open) triangles in (a) and (c) denote the phase boundaries, $H_{\text{A}1}$ and $H_{\text{A}2}$ ($H_{\text{c}1}$, $H_{\text{c}2}$, and H_{P}), which are determined from the dM/dH and dL/dH anomalies, respectively. The dashed gray lines in (b) and (d) trace the boundaries of A-phase.$

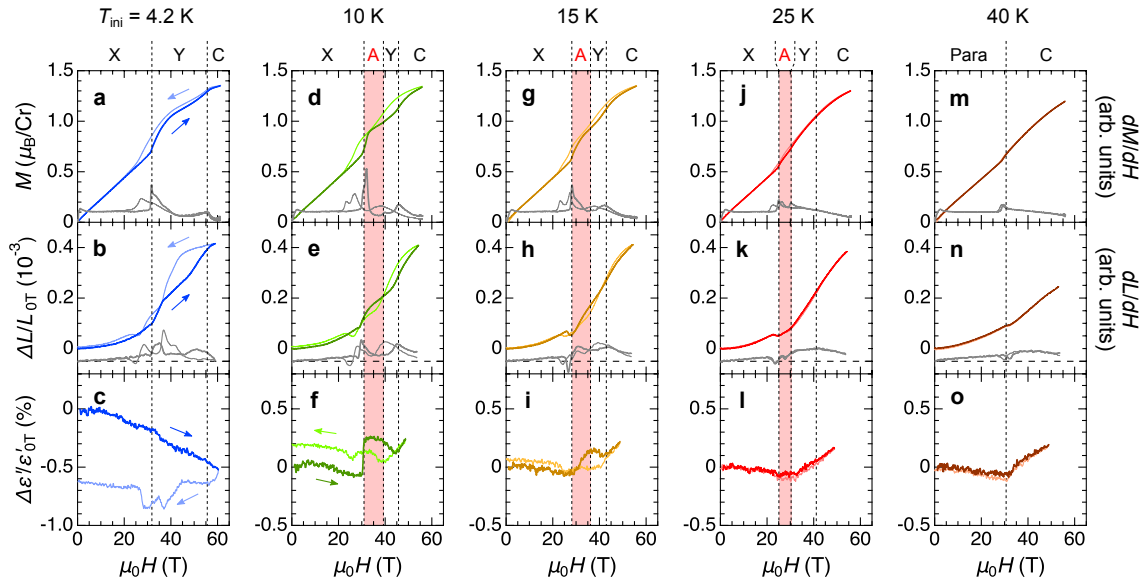


Fig. 4: Anomalous magnetostriuctive and magnetocapacitive effects in A-phase of CuInCr₄S₈. Top, middle, and bottom panels show the magnetic-field dependence of magnetization, longitudinal magnetostriction, and magnetocapacitance, respectively, for $T_{\text{ini}} = 4.2 \text{ K}$ (**a-c**), 10 K (**d-f**), 15 K (**g-i**), 25 K (**j-l**), and 40 K (**m-o**). The field-derivatives of magnetization and magnetostriction are also shown by gray lines in the right axes. The magnetocapacitance was measured along the field direction at a frequency of 50 kHz. The thick (thin) lines correspond to the data in field-elevating (descending) processes. The phase boundaries are roughly drawn by dashed black lines, which are determined from the data in the field-elevating process.

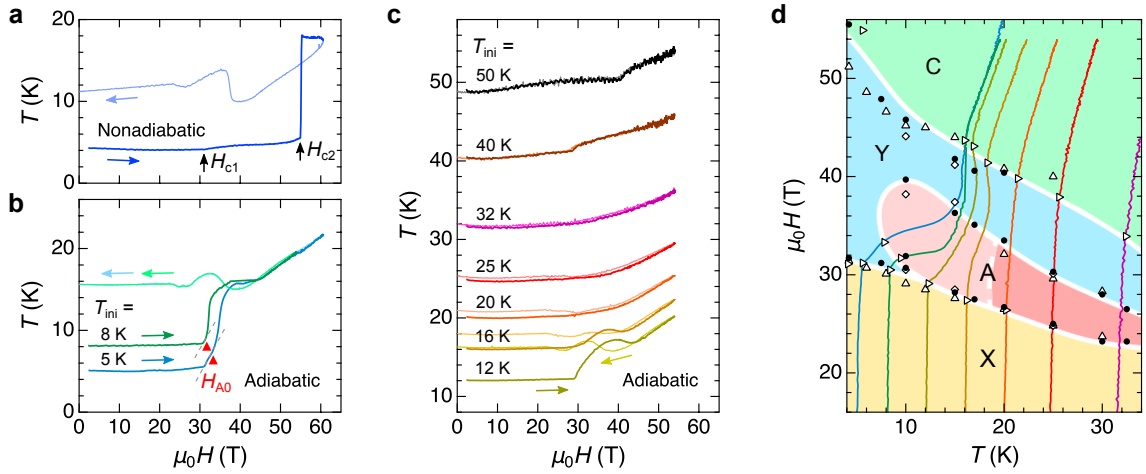


Fig. 5: Temperature change of CuInCr₄S₈ in pulsed magnetic fields. $T(H)$ curve obtained under the nonadiabatic condition at $T_{\text{ini}} = 4.2$ K (**a**) and under the adiabatic condition at various T_{ini} 's (**b-d**). In (**a-c**), the thick (thin) lines correspond to the data in the field-elevating (descending) process. In (**b**), the $T(H)$ curves in field-descending processes for $T_{\text{ini}} = 5$ and 8 K completely overlap with each other. Dashed gray lines are guides to the eye to make it easier to see the possible phase transition from Y- to A-phase at H_{A0} (denoted by red triangles). In (**d**), $T(H)$ curves in field-elevating processes are plotted on the H - T phase diagram shown in Fig. 1(d), focusing on the parameter region where multi-stage phase transitions take place.

Supplementary Information for Complex magnetic phase diagram with a small phase pocket in a three-dimensional frustrated magnet $\text{CuInCr}_4\text{S}_8$

M. Gen^{1,2*}, H. Ishikawa¹, A. Ikeda¹, A. Miyake¹, Z. Yang¹, Y. Okamoto³, M. Mori³, K. Takenaka³, T. Kurumaji², Y. Tokunaga², T. Arima², M. Tokunaga¹, K. Kindo¹, Y. H. Matsuda¹, and Y. Kohama¹

¹ *Institute for Solid State Physics, University of Tokyo, Kashiwa 277-8581, Japan*

² *Department of Advanced Materials Science, University of Tokyo, Kashiwa 277-8561, Japan*

³ *Department of Applied Physics, Nagoya University, Nagoya 464-8603, Japan*

*Correspondence is addressed to M.G. (E-mail: gen@edu.k.u-tokyo.ac.jp)

Supplementary Note 1. Powder X-ray diffraction patterns of Samples #1 and #2

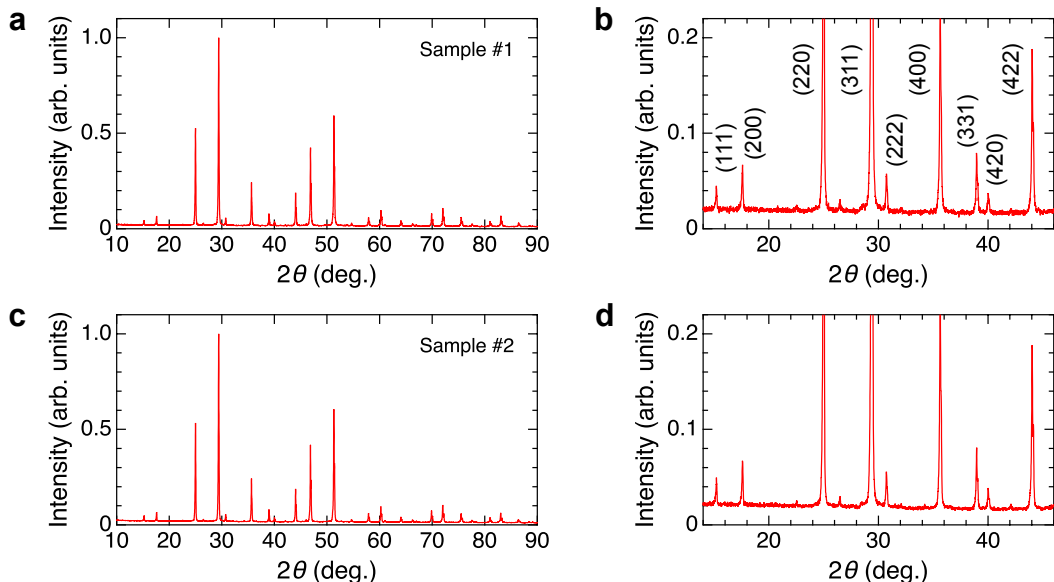


Fig. S1: Powder X-ray diffraction (XRD) patterns of $\text{CuInCr}_4\text{S}_8$ at room temperature for Sample #1 (**a**, **b**) and Sample #2 (**c**, **d**). (**b**) and (**d**) are enlarged views of (**a**) and (**c**) in the region of $14^\circ \leq 2\theta \leq 46^\circ$, respectively. The vertical axis is normalized by the strongest (311) peak intensity located at around 30° . There is no apparent difference between the two patterns, including the (200) and (420) peaks, which are forbidden for $Fd\bar{3}m$ but allowed for $F\bar{4}3m$ space group. The structural parameter of Sample #2 has been identified as shown in Ref. [S1].

Supplementary Note 2. Magnetization and magnetostriction curves for Sample #2

Figure S2 summarizes the magnetization and magnetostriction data measured for Sample #2 at various initial temperatures (T_{ini} 's) in pulsed magnetic fields of up to 57 T. It can be seen that the observed phase transitions are much blunt compared to those for Sample #1 (Fig. 3) although all the critical fields H_{c1} , H_{c2} , H_{A1} , H_{A2} and H_p are consistent with each other. Furthermore, an additional dM/dH hump is observed at around $\mu_0 H_{c0} \approx 25$ T for $1.4 \leq T_{\text{ini}} \leq 20$ K (Figs. S2a and S2b). These observations signal the dispersion in the strength of exchange interactions caused by a tiny amount of crystallographic disorder in Sample #2.

Note again that the magnetic long-range ordering temperature for Sample #2 ($T_N = 32$ K) is lower than that for Sample #1 ($T_N = 35$ K). This would be for the same reason as mentioned above. We found that T_N changes slightly from synthesis to synthesis, and the magnetic properties are very sensitive to the sample quality. As far as we have tried, Sample #1 adopted as the main data seems of the highest quality.

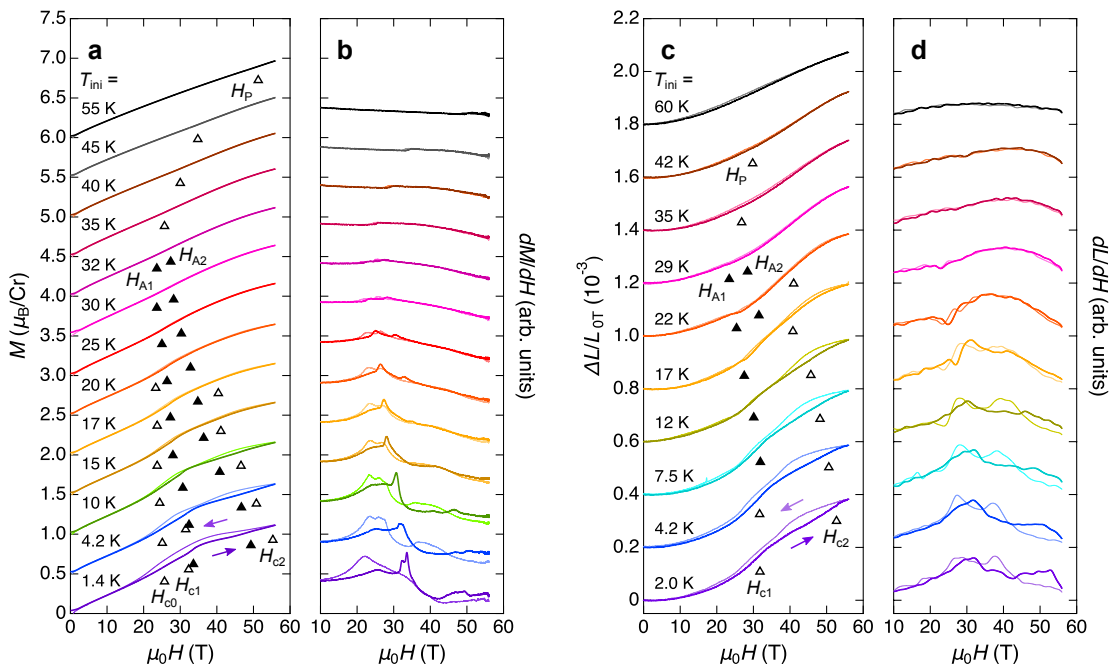


Fig. S2: (a) Magnetization, (b) its field-derivative, (c) longitudinal magnetostriction, and (d) its field-derivative of $\text{CuInCr}_4\text{S}_8$ as a function of magnetic field measured at various initial temperatures T_{ini} for Sample #2 ($T_N = 32$ K). The thick (thin) lines correspond to the data in the field-elevating (descending) process. All the data except for the lowest-temperature one are shifted upward for clarity. The filled (open) triangles in (a) and (c) denote the phase boundaries, H_{A1} and H_{A2} (H_{c0} , H_{c1} , H_{c2} , and H_p), which are determined from the dM/dH and dL/dH anomalies, respectively.

Supplementary Note 3. *H-T* phase diagram for Sample #2

Figure S3 shows the magnetic-field-versus-temperature (*H-T*) phase diagram for Sample #2, which should have more crystallographic disorder than Sample #1 as discussed in Supplementary Note 2. The phase diagram is obtained from the magnetic susceptibility data up to 7 T and the high-field magnetization and magnetostriction data in the field-elevating process (Fig. S2). The overall feature is similar with the *H-T* phase diagram for Sample #1 (Fig. 1d), except for A-phase and X'-phase. The existence of X'-phase would not be an intrinsic property of CuInCr₄S₈ with the perfect breathing pyrochlore lattice. Importantly, A-phase seems to further extend down to below 1.4 K, indicating that the appearance of A-phase is an intrinsic property and its metastability is quite sensitive against the sample quality.

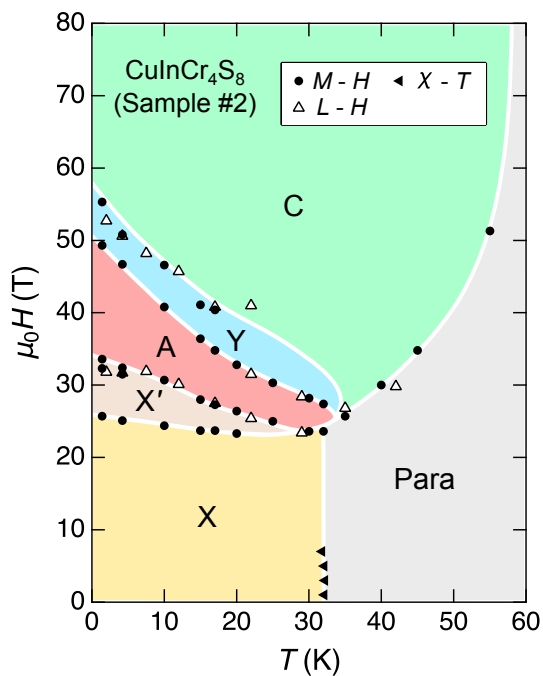


Fig. S3: Magnetic-field-versus-temperature phase diagram for Sample #2.

Supplementary Note 4. DM interactions in the breathing pyrochlore lattice with

$$J > 0 \text{ and } J' < 0$$

For the regular pyrochlore lattice, Dzyaloshinskii-Moriya (DM) interactions can be present on all the nearest-neighbor (NN) bonds because of the absence of an inversion center at the middle point between NN sites [S2,S3]. As pointed out in Ref. [S4], there are two possible ways to locate DM vectors, both of which resolve the macroscopic degeneracy caused by geometrical frustration and lead to the magnetic long-range order: one selects the “all-in-all-out” spin configuration whereas the other selects the coplanar one as the ground state.

When one introduces the breathing bond alternation on the pyrochlore lattice, DM vectors with different strength and sign would be allowed in the large and small tetrahedra. In the present case of AFM $J > 0$ and strong FM exchange $J' < 0$, however, the effects of DM vectors within the large tetrahedra should be negligible, so that there are eventually two possible ways to locate effective DM vectors, which are depicted on the effective FCC lattice in Fig. S4. The degeneracy within the type-I magnetic order with $\mathbf{q}=(1\ 0\ 0)$ cannot be resolved by DM interactions in either case. Therefore, we conclude that DM interactions are not responsible for the appearance of X-phase.

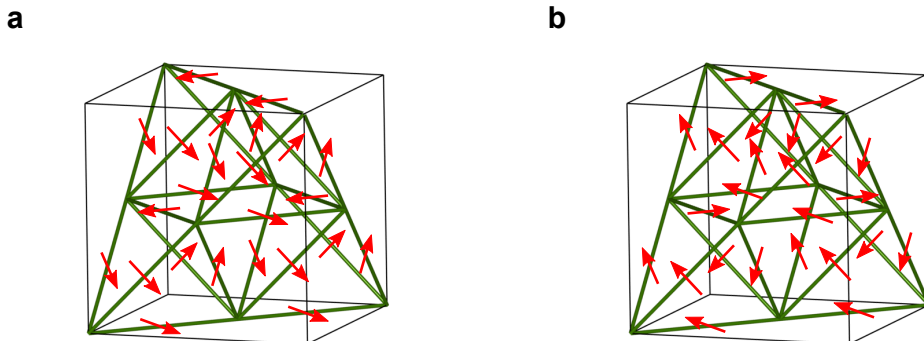


Fig. S4: Two possible DM vectors on the effective FCC lattice.

Supplementary Note 5. Magnetic entropy changes below T_N at zero field

We here estimate the temperature dependence of the magnetic entropy in $\text{CuInCr}_4\text{S}_8$ at zero field based on the observed $C/T-T$ curve (Fig. 2b) and compare the results with that in the typical Cr spinel antiferromagnet CdCr_2O_4 . For estimating the lattice contribution, we adopt the Debye model due to the lack of a suitable nonmagnetic reference compound. The calculated lattice contributions with the Debye temperature $\Theta_D = 390, 440$, and 500 K are shown in Fig. S5a. The magnetic entropy at $T_N = 35$ K is obtained as $S_M = 4 \sim 5 \text{ JK}^{-1}/\text{mol-Cr}$ (Fig. S5b), which is less than half of Rln4 , indicating that the magnetic short-range order develops above T_N . In contrast to $\text{CuInCr}_4\text{S}_8$, the $C/T-T$ curve for CdCr_2O_4 exhibits a sharp peak at $T_N = 7.8$ K (Fig. S5c) [S5], where a structural transition also takes place [S6]. A similar sharp peak in C/T associated with a strong entropy drop is the universal property in other Cr spinels [S7] and the breathing pyrochlore families [S1,S8].

Figure S5d visualizes the difference in the way of the magnetic entropy release below T_N between $\text{CuInCr}_4\text{S}_8$ and CdCr_2O_4 . As readily seen, the entropy reduction just below T_N is much slower for $\text{CuInCr}_4\text{S}_8$ than for CdCr_2O_4 : $S_M(0.8 T_N)/S_M(T_N) \sim 0.64$ for $\text{CuInCr}_4\text{S}_8$, whereas $S_M(0.8 T_N)/S_M(T_N) \sim 0.35$ for CdCr_2O_4 . This strongly supports the existence of spin fluctuation in X-phase for $\text{CuInCr}_4\text{S}_8$, which would be originated from the magnetic frustration inherent to the effective FCC lattice.

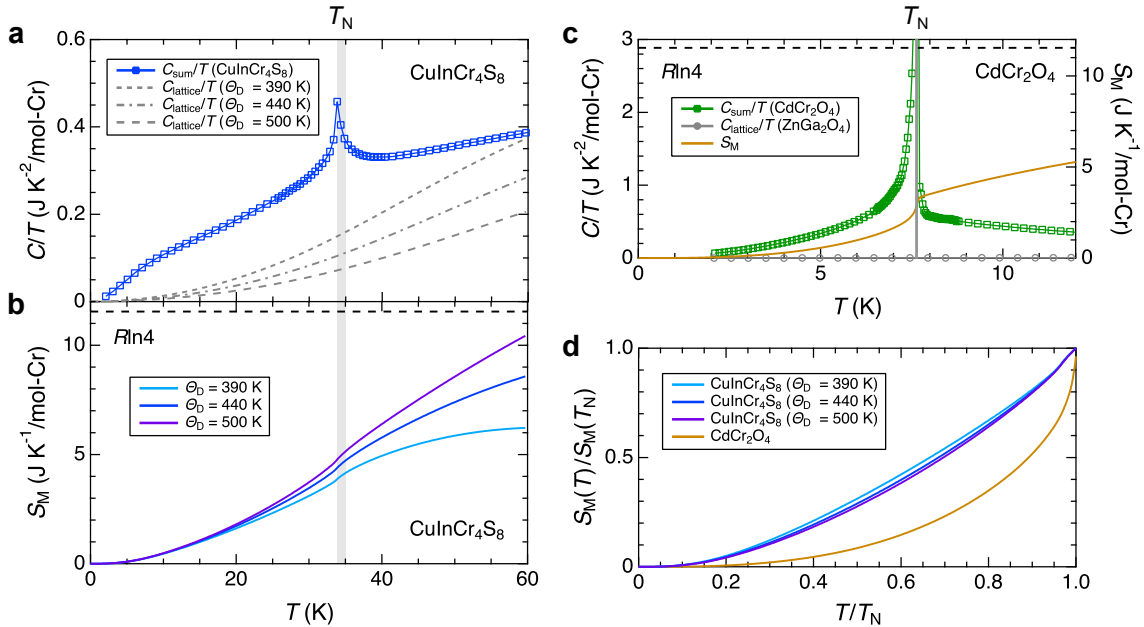


Fig. S5: (a) Temperature dependence of the specific heat divided by temperature C_{sum}/T for $\text{CuInCr}_4\text{S}_8$ at 0 T (Fig. 2b) and the estimated lattice contribution C_{lattice}/T based on the Debye model with $\Theta_D = 390, 440$, and 500 K. (b) Temperature dependence of the magnetic entropy for $\text{CuInCr}_4\text{S}_8$ calculated by integrating $(C_{\text{sum}} - C_{\text{lattice}})/T$. (c) Temperature dependence of the specific heat divided by temperature for CdCr_2O_4 and the nonmagnetic ZnGa_2O_4 at 0 T (left), and the calculated magnetic entropy for CdCr_2O_4 (right). The data are taken from Ref. [S5]. (d) Relative magnetic entropy changes below T_N for $\text{CuInCr}_4\text{S}_8$ and CdCr_2O_4 .

Supplementary Note 6. Phase transitions during the field-descending process

We here mention the nature of the successive phase transitions of CuInCr₄S₈ for the field-descending process. Figure S6 shows the magnetization, magnetostriction, magnetocapacitance, and magnetocaloric effect (MCE) curves in the field-descending process obtained under the nonadiabatic condition for Sample #1. The latter three data are taken at $T_{\text{ini}} = 4.2$ K, while the magnetization are taken at $T_{\text{ini}} = 7.5$ K. As discussed in the main text, CuInCr₄S₈ significantly suffers from the MCE by the pulsed field application, so that the sample temperature during the field-descending process would be largely different from T_{ini} and dependent on the experimental setup. Although the exact sample temperature is unknown in Figs. S6a-S6c, it is expected to be roughly as shown in Fig. S6d.

Remarkably, there exist at least four anomalies signaling phase transitions. Similar to the case of the field-elevating process, the low-field phase below ~ 23 T and the high-field phase above ~ 44 T should correspond to X- and C-phases, respectively. For the intermediate-field region, several kinds of magnetic phases beyond A- and Y-phases seem to appear accompanied by considerable magnetostrictive and magnetocapacitive responses as well as moderate entropy changes. Here, we tentatively define them as phase I, II, and III from the high-field side. Judging from the dip structure of $\Delta L/L_{0T}$ and the sharp magnetocapacitive anomaly around the phase boundary between phases II and III, a large modification of the magnetic structure with the reconstruction of q -vector would occur.

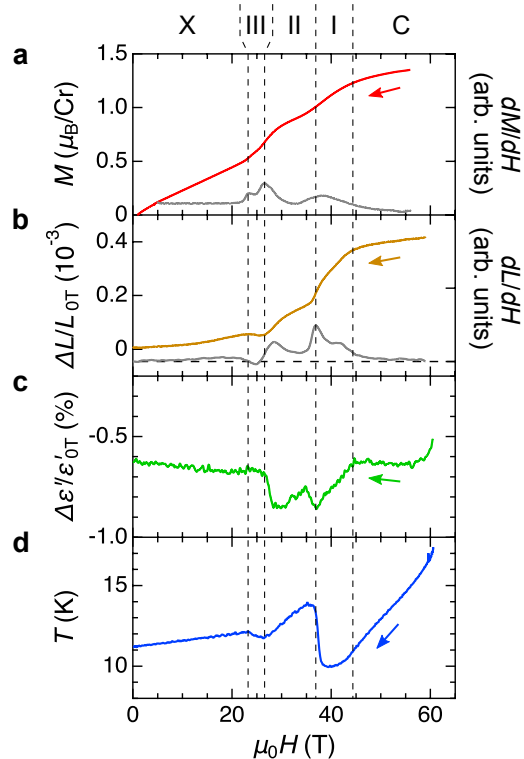


Fig. S6: (a) Magnetization, (b) longitudinal magnetostriction, (c) magnetocapacitance, and (d) magnetocaloric effect curves in the field-descending process measured for Sample #1. The field-derivatives of magnetization and magnetostriction are also shown by gray lines in the right axes.

References

- [S1] Y. Okamoto, M. Mori, N. Katayama, A. Miyake, M. Tokunaga, A. Matsuo, K. Kindo, and K. Takenaka, Magnetic and Structural Properties of A-Site Ordered Chromium Spinel Sulfides: Alternating Antiferromagnetic and Ferromagnetic Interactions in the Breathing Pyrochlore Lattice, *J. Phys. Soc. Jpn.* **87**, 034709 (2018).
- [S2] I. Dzyaloshinskii, A thermodynamic theory of “weak” ferromagnetism of antiferromagnetics, *J. Phys. Chem. Solids* **4**, 241-255 (1958).
- [S3] T. Moriya, New Mechanism of Anisotropic Superexchange Interaction, *Phys. Rev. Lett.* **4**, 228 (1960).
- [S4] M. Elhajal, B. Canals, R. Sunyer, and C. Lacroix, Ordering in the pyrochlore antiferromagnet due to Dzyaloshinsky-Moriya interactions, *Phys. Rev. B* **71**, 094420 (2005).
- [S5] S. Kitani, M. Tachibana, N. Taira, and H. Kawaji, Thermal study of the interplay between spin and lattice in CoCr_2O_4 and CdCr_2O_4 , *Phys. Rev. B* **87**, 064402 (2013).
- [S6] L. Rossi, A. Bobel, S. Wiedmann, R. Küchler, Y. Motome, K. Penc, N. Shannon, H. Ueda, and B. Bryant, Negative Thermal Expansion in the Plateau State of a Magnetically Frustrated Spinel, *Phys. Rev. Lett.* **123**, 027205 (2019).
- [S7] M. C. Kemei, P. T. Barton, S. L. Moffitt, M. W. Gaulois, J. A. Kurzman, R. Seshadri, M. R. Suchomel, and Y. Kim, Crystal structures of spin Jahn-Teller-ordered MgCr_2O_4 and ZnCr_2O_4 , *J. Phys.: Condens. Matter* **25**, 326001 (2013).
- [S8] Y. Okamoto, G. J. Nilsen, J. P. Attfield, and Z. Hiroi, Breathing Pyrochlore Lattice Realized in A-Site Ordered Spinel Oxides $\text{LiGaCr}_4\text{O}_8$ and $\text{LiInCr}_4\text{O}_8$, *Phys. Rev. Lett.* **110**, 097203 (2013).